Cancer Imaging (2010) **10,** S112–S123
DOI: 10.1102/1470-7330.2010.9030

CI

e-med
www.e-med.org.uk

DW-MRI of the urogenital tract: applications in oncology

G. Petralia[a,b] and H.C. Thoeny[a]

[a]Institute of Diagnostic, Pediatric and Interventional Radiology, University Hospital of Bern, Inselspital, Freiburgstrasse 10, CH-3010 Bern, Switzerland; [b]Department of Radiology, European Institute of Oncology, Via Ripamonti 435, 20141 Milan, Italy

Corresponding address: Harriet C. Thoeny, MD, Institute of Diagnostic, Pediatric and Interventional Radiology, University Hospital of Bern, Inselspital, Freiburgstrasse 10, CH-3010 Bern, Switzerland.
Email: harriet.thoeny@insel.ch

Abstract

Diffusion-weighted magnetic resonance imaging (DW-MRI) appears to hold promise as a non-invasive imaging modality in the detection of early microstructural and functional changes of different organs. DW-MRI is an imaging technique with a high sensitivity for the detection of a large variety of diseases in the urogenital tract. In kidneys, DW-MRI has shown promise for the characterization of solid lesions. Also in focal T1 hyperintense lesions DW-MRI was able to differentiate hemorrhagic cysts from tumours according to the lower apparent diffusion coefficient (ADC) values reported for renal cell carcinomas. Promising results were also published for the detection of prostate cancer. DW-MRI applied in addition to conventional T2-weighted imaging has been found to improve tumour detection. On a 3 T magnetic resonance unit ADC values were reported to be lower for tumours compared with the normal-appearing peripheral zone. The combined approach of T2-weighted imaging and DW-MRI also showed promising results for the detection of recurrent tumour in patients after radiation therapy. DW-MRI may improve the performance of conventional T2-weighted and contrast-enhanced MRI in the preoperative work-up of bladder cancer, as it may help in distinguishing superficial from muscle invasive bladder cancer, which is critical for patient management. Another challenging application of DW-MRI in the urogenital tract is the detection of pelvic lymph node metastases. As the ADC is generally reduced in malignant tumours and increased under inflammatory conditions, reduced ADC values were expected in patients with lymph node metastases.

Keywords: *Diffusion-weighted magnetic resonance imaging; tumours; kidney; bladder; prostate; lymph nodes.*

Introduction

Conventional magnetic resonance imaging (MRI) and computerized tomography (CT) are excellent techniques for imaging the urogenital tract. Kidney tumours including transitional cell carcinomas (TCCs) are routinely staged with CT or in special cases with MRI. Local staging of prostate tumours can be performed only with MRI, but CT is used in the search for distant metastases. These techniques, however, only provide morphological information on tumours; they lack information related to tumour micro-architecture and biology.

Diffusion-weighted magnetic resonance imaging (DW-MRI) measures microscopic mobility of water molecules in the tissues. This mobility, which is classically called Brownian motion, is caused by thermal motion and is highly influenced by the cellular environment of water. Thus, findings on DW-MRI can reflect biologic abnormalities of the underlying tissues. The first clinical applications of DW-MRI were reported in the brain in the 1990s[1]. In the meantime DW-MRI is state-of-the-art for the diagnosis of an acute stroke, as microstructural changes observed on DW-MRI precede morphological changes on conventional MRI or CT[2,3].

In the past, the use of DW-MRI for imaging the abdomen was limited by a number of technical challenges, mainly related to physiological motion artefacts (bowel, cardiac and respiratory motion) and the heterogeneous composition of the organs. However, the latest technological developments have improved the quality of DW-MRI sequences for the abdomen[4] and there is now a broad spectrum of abdominal

1470-7330/10/000001 + 12

applications, including functional assessment of different organs (e.g. the kidneys), tissue characterization, as well as prediction and monitoring of treatment response in tumours[5].

The present review outlines the basic principles of DW-MRI and its applications in the urogenital tract (kidney, bladder, prostate) are discussed with the main focus on oncology including pelvic lymph node metastases.

Basics of DW-MRI

The most commonly used DW-MRI sequence is based on the use of 2 equal-sized gradients, separated by a 180° radiofrequency (RF) pulse. The effect of these 2 gradients on water molecules is different according to their movement. In stationary water molecules that have not moved substantially between the first and second gradient, the extra rotation induced by the second gradient will be identical to the first one and all of them will be in phase at the end of the second gradient, generating virtually a high signal. In contrast, in non-stationary water molecules that have moved between the first and second gradient, the second extra rotation will no longer be identical to the first, and the molecule will be out of phase, generating a lower signal than an in-phase configuration. The signal loss after the second gradient is also dependent on the strength of the gradient (G) applied. The amount of diffusion sensitizing applied is usually indicated by the b value, which is given by $b = \gamma^2 \times G^2 \times \delta^2 \times (\Delta - \delta/3)$, where γ is the gyromagnetic ratio, G the strength of the gradient used, δ is the duration of the gradient and Δ is the time between the 2 gradients.

This signal loss as a function of the b value (or diffusion weighting) usually shows an exponential behaviour, which is generally displayed in a logarithmic scale. By applying the following formula ($S_i = S_0 \times \exp(-b_i \times \mathrm{ADC})$, where S_i is the signal intensity measured using a b value b_i and S_0 is the signal intensity for $b = 0$ s/mm^2. It is then possible to calculate the apparent diffusion coefficient (ADC) of water molecules[5], which is usually displayed in pixel-by-pixel maps (ADC maps) in a grey scale (higher and lower ADC values in colour shades of light and dark grey, respectively).

All moving molecules in a tissue volume induce a signal loss. This means that not only the diffusion of water molecules in the extracellular extravascular space but also cellular diffusion as well as intravascular perfusion contribute to the calculation of the ADC value[2,4,6,7]. However, the effect of the movement of water molecules on the ADC value is inversely related to their speed at the moment of the MR examination. Using low b values (typically up to 100–150 s/mm^2), the fastest moving spins have the strongest effect. The origin of these fast spins can most likely be attributed to microperfusion and microcirculation effects and this phenomenon, also known as the intravoxel incoherent motion, has been used to assess tissue perfusion[2,4,6,7]. Using higher b values, the fastest moving spins have already lost their signal; therefore, the effect of the slower movements such as the Brownian displacement of extra- and intracellular molecules and trans-membranous transport can be assessed[8]. Whenever the micro-architecture of a tissue is changed, either with respect to the blood vessel density, to the addition and/or removal of structural inhibitors, or, most importantly, to the different ratio of extracellular extravascular space over the intracellular space, this can be detected using DW-MRI, provided an optimal choice of b values is selected. For example, a reduced ADC has been observed in most types of malignant tumours as a result of the decrease in extracellular extravascular space[8].

The selection of an appropriate imaging sequence is essential for DW-MRI. In theory, any imaging sequence can be adapted with bipolar gradients to allow the assessment of water molecule diffusion. However, the fastest and most often used sequence is a single-shot echo-planar imaging (EPI) sequence, which is a gradient echo-based technique and therefore has inherent problems with susceptibility, especially when many air–tissue boundaries are present. Also, movement artefacts tend to have a stronger effect in gradient echo acquisitions. As both factors are more pronounced in abdominal applications, some researchers tend to use alternative acquisition schemes such as single-shot turbo-spin-echo, steady-state free precession, multi-shot EPI and line scan diffusion-weighted imaging.

Technical requirements

Different sequences have been described for DW-MRI of the urogenital tract.

Breath-hold sequences are fast (15–20 s) and minimally affected from pulsatility and motion artefacts, but are limited in coverage, have a low signal-to-noise ratio (SNR) (as they are performed with few averages) and only allow application of a few b values.

Free breathing or respiratory triggered sequences are now increasingly performed in the urogenital tract. They allow for full region coverage and motion or pulsatility artefacts are cancelled out with the use of multiple averages, which also increase the SNR. The time of acquisition for such sequences, however, is longer (>5 min) than that required for breath-hold sequences. Both the above-mentioned DW-MRI sequences are usually acquired before contrast medium administration. Imaging of the kidney is often performed in the coronal plane, whereas imaging of the pelvis should be performed in the transverse plane.

The choice of b values depends on the clinical indication. Only higher b values enable an estimate of true diffusion of water molecules; whereas a combination of high and low b values cannot separate the contribution of perfusion and diffusion in tissues, generating higher ADC values.

The number of *b* values included in a sequence has also to be decided according to the purpose of the study. The higher the number of *b* values used, the more precise is the ADC fit; on the other hand, the time of acquisition increases according to the number of *b* values applied. Therefore, multiple *b* values are required for bi-exponential fitting of the signal intensity curve, in order to separate the contribution of perfusion from that of diffusion in the calculation of ADC; in contrast, in the clinical routine an acceptable ADC fit can usually be obtained with 3–4 *b* values[9]. Typical parameters for a free breathing axial EPI sequence adapted for imaging of the urogenital tract with a 1.5 T scanner include slice thickness 5–6 mm with no intersection gap, field of view (FOV) 360–400 mm, matrix 104–112/256, number of slices 40–46, repetition time from 5000 to 7000 ms, a echo time as low as possible (65–68 ms), at least 3 *b* values (e.g. 0, 500, 1000 s/mm^2), parallel imaging (acceleration factor 2), EPI factor 75–112, bandwidth 1800 Hz/pixel, averages 4–5, acquisition time approximately 4 min.

The administration of an anti-peristaltic agent such as glucagon or hyoscine-*N*-butyl bromide helps to minimise bowel motion and consequent susceptibility artefacts in the pelvis; it is therefore recommended for DW-MRI of the pelvis.

Magnetic susceptibility artefacts from hip prostheses usually impair the quality of EPI-based DW-MRI sequences, thus limiting its application in these patients.

Image analysis

The qualitative analysis of DW-MR images can be performed by visual assessment. Tissues present a different attenuation with increasing *b* values, which is related to tissue cellularity, to the integrity of cell membranes and to the tortuosity of the extracellular space[5,10]. Generally, at higher *b* values (e.g. >800 s/mm^2), cellular tissue (e.g. tumour tissue) shows less signal attenuation (being hyperintense) than free fluid or necrotic/cystic components of a tumour (being hypointense). However, the interpretation of DW-MR images alone may have limitations. For example, due to the T2 shine-through effect, some normal tissues (e.g. the peripheral zone (PZ) of the prostate) show high signal intensity even in the higher *b* value DW-MR images. This occurs because the signal intensity on the high *b* value DW-MR images depends not only on the diffusion of water molecules but also on the intrinsic tissue T2-relaxation time; a DW-MRI EPI sequence is an adaptation from a T2-weighted spin-echo sequence.

The easiest method to avoid misinterpretation because of the T2 shine-through effect is to compare the high *b* value DW-MR image with the corresponding ADC map[10]. A tissue with a significant T2 shine-through effect typically shows high signal intensity on the high *b* value image, but returns a high ADC value, displayed in colour shades of light grey on the corresponding ADC maps (Fig. 1). Such a combined interpretation of DW-MR images and ADC maps is therefore strongly advocated for the urogenital tract, leading to a new radiological interpretation of lesions. High signal intensity on the high *b* value DW-MR images and colour shades of dark grey on ADC maps indicate a cellular tissue, including malignancy within the differential diagnosis (Fig. 2); however, abscesses might also be cellular, with similar appearance. When a lesion shows low signal intensity in low *b* value images and colour shades of light grey on ADC maps, it is mostly related to cystic or necrotic components (Fig. 2). When a lesion shows low signal intensity on high *b* value DW-MR images and colour shades of dark grey on the ADC maps in grey scale, some conditions could be considered, including suppressed macroscopic fatty tissue, as well as susceptibility artefacts (e.g. iron deposition) (Fig. 3).

The quantitative analysis of DW-MR images can be performed by calculating the ADC values of tissues. A region of interest (ROI) is manually drawn along tumour margins, in each section where it is present. The ROI is generally drawn on DW-MR images and then copied on ADC maps, as tumour margins can be difficult to identify on ADC maps. In renal lesions, which might show both solid and necrotic/cystic components, it might be more precise to draw different ROIs on the 2 different components. The simplest and most frequently used method to quantify the tumour ADC is by using summary statistics; the mean or median ADC of the ROI can be easily obtained and reported. However, the value obtained does not reflect the distribution of the ADC values within the ROI, thus providing a poor assessment of tumour heterogeneity. The ADC values can also be analysed on a voxel-by-voxel basis, which allows the assessment of the individual voxel values within an ROI. The distribution of the ADC values within the ROI can be displayed by histograms, which better reflect tumour heterogeneity.

DW-MRI in different urogenital organs

Kidney

CT and MRI easily identify a renal neoplasm and usually allow the diagnosis of a neoplastic process when contrast enhancement is present. However, the difference between complicated cysts and cystic renal cell carcinoma (RCC) or between an oncocytoma and an RCC can be challenging. In these cases, additional information might be helpful for further characterization of unclear cystic or solid lesions.

As a general rule, lower ADC values are expected in solid lesions, reflecting impeded diffusion of water molecules as a result of cellular density, compared with those in cystic lesions. This has been confirmed by several studies, which demonstrated a higher ADC in simple

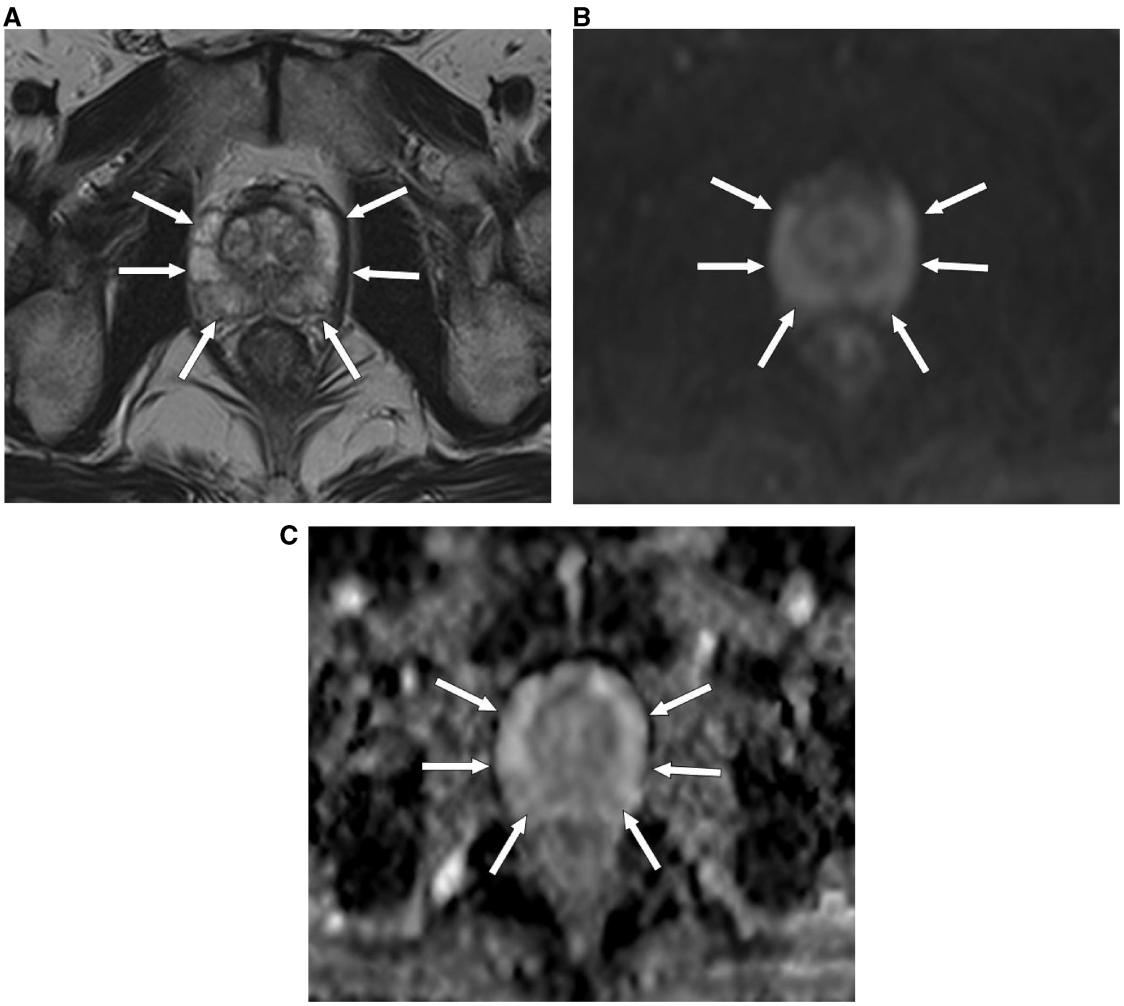

Figure 1 **MRI (at 1.5 T) of a 66-year-old male patient with a normal prostate. (A) Axial T2-weighted image shows high signal intensity in the PZ of the prostate (arrows). (B) DW-MR image at a *b* value of 900 s/mm^2 shows high signal intensity in the PZ of the prostate, as a result of the T2 shine-through effect (arrows). (C) The PZ of the prostate returns a high ADC value, represented by colour shades of light grey (arrows).**

cysts than in normal parenchyma and in solid lesions[11,12].

Using *b* values of 0, 500, and 1000 s/mm^2, Zhang *et al.*[13] demonstrated significantly lower ADC values in the cystic/necrotic portions of a neoplasm compared with simple cysts: 2.21 ± 0.63 versus 3.26 ± 0.61 ($P < 0.05$). The only study that compared the ADC values of Bosniak cysts showed an ADC of 1.83 ± 0.85 for complicated cysts (category III–IV from Bosniak); an ADC of 2.78 ± 0.45 was observed for category I[14]. These encouraging results, however, need to be further assessed in larger prospective studies.

Another diagnostic challenge for conventional cross-sectional imaging is the differentiation between an oncocytoma and a solid RCC. Promising results have been reported in a recent study, which demonstrated that renal oncocytomas had a significantly higher ($P = 0.0097$) ADC value compared with that of solid RCCs (mean ADC values for *b* values of 0, 400, and 800 s/mm^2 were $1.91 \times 10^{-3} \pm 0.97$ s/mm^2 versus $1.54 \times 10^{-3} \pm 0.69$ s/mm^2, respectively)[14].

The potential of DW-MRI in the characterization of focal renal lesions is of utmost importance in patients with renal insufficiency, in view of the recently reported concerns regarding the risk of development of nephrogenic systemic fibrosis (NSF)[15–18]. In a recent study including 109 renal lesions (81 benign lesions and 28 RCCs), contrast-enhanced MRI performed better than DW-MRI for the diagnosis of RCCs, but the authors concluded that DW-MRI alone is currently a reasonable alternative to contrast-enhanced MR or CT imaging for the diagnosis of malignant renal neoplasms in patients with renal insufficiency and/or are at risk for NSF[14] or contrast material–induced nephropathy[19]. In a recently published study, the performance of DW-MRI was equivalent to that of enhancement ratio in the characterization

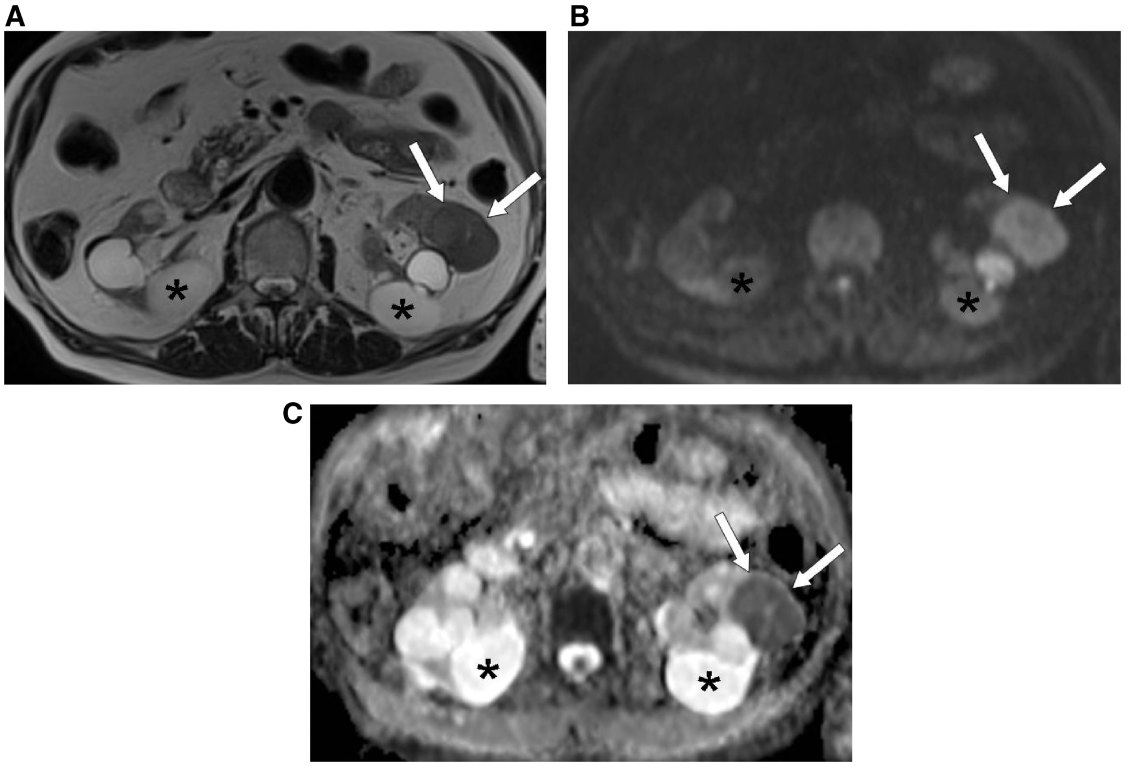

Figure 2 **MRI (at 1.5 T) of a 79-year-old patient with an RCC in the left kidney (arrows). (A) Axial T2-weighted MR image shows intermediate signal intensity of the RCC, which is comparable with that of normal parenchyma, and high signal intensity for the multiple bilateral simple cysts (asterisk). (B) DW-MR image at a *b* value of 900 s/mm^2 shows high signal intensity of the RCC (arrows) and low signal intensity of the simple cysts (asterisk). (C) In the ADC map the RCC is clearly visualized as an area of impeded diffusion (arrows), represented by colour shades of dark grey, in contrast with the normal parenchyma of the left kidney and with the simple cysts (asterisk), which return colour shades of intermediate and light grey, respectively.**

	Cellular tissue, tumour	Cystic/necrotic tissue	T2 shine through effect	Macroscopic fat, artefacts
Signal intensity (high b-values images)		■		■
Colour (ADC maps in grey scale)	■			■

Figure 3 **Qualitative analysis of the common patterns in DW-MRI, using high *b* value images and corresponding ADC maps in grey scale (colour shades of light grey correspond to higher ADC values, whereas colour shades of dark grey correspond to lower ADC values). Boxes in white indicate high signal intensity on high *b* value images and high ADC values. Boxes in black indicate low signal intensity on high *b* value images and low ADC values.**

of non–fat-containing T1 hyperintense renal lesions; both methods had lower sensitivity than image subtraction, however without reaching significance[20]. The results of this study further confirm the role of DW-MRI as a valid alternative to contrast-enhanced imaging by MR or CT, even in the above-mentioned clinical setting, which is traditionally challenging for any imaging modality.

Bladder

The most common type of bladder cancer is TCC. At the time of diagnosis, more than 70% of bladder cancers are superficial (stage T1 or lower), confined to the subepithelial connective tissue[21–23]; the remaining bladder cancers are muscle invasive (stage T2) or extend beyond the bladder (stage T3 or T4). Distinguishing

superficial from muscle invasive bladder cancer is critical for patient management, because the treatment options differ considerably. Superficial tumours are treated with bladder sparing treatments, including transurethral resection (TUR) with or without adjuvant intravesical chemotherapy or photodynamic therapy[24]. A radical cystectomy with lymphadenectomy, radiation therapy, chemotherapy, or a combination is required for muscle invasive bladder cancers[25]. Cystoscopy and TUR can underestimate the local extent of the disease in the bladder[26]. Therefore, preoperative imaging able to precisely differentiate between the 2 categories of bladder cancer would have a great clinical impact.

Conventional MRI can visualize bladder tumours, which appear slightly hyperintense relative to muscle on T2-weighted sequences and isointense relative to muscle on T1-weighted sequences[23]. T2a and T2b tumours can occasionally be differentiated when on a T2-weighted sequence the hypointense band (corresponding to the muscle) is preserved, corresponding to T2a tumours[23]. Macroscopic extravesical extension (T3b) of the tumour can be seen on conventional MRI, as a result of the presence of an irregular, ill-defined outer bladder wall and soft-tissue nodules or fat stranding in the surrounding perivesical fat[27]. However, conventional MRI techniques cannot resolve the various bladder wall layers accurately, thereby seriously limiting the accuracy of T staging, particularly in distinguishing among muscle invasive (stage T2 or higher) and superficial (stage T1 or lower) tumours.

Some authors observed that DW-MRI is superior to T2-weighted MRI in staging of organ-confined tumours ($\leq$T2)[28] and may have high specificity (93%) for the detection of invasive urinary bladder tumours[29]. The additional value of DW-MRI for differentiating stage Tis to T1 tumours from T2 to T4 tumours has been investigated. In a recent study DW-MRI had increased accuracy from 88% up to 98% when performed in addition to T2-weighted and contrast-enhanced imaging, and from 79% up to 96% when performed in addition to T2-weighted imaging alone[30]. Furthermore, the excellent specificity for muscle invasion (100%) that has been observed when DW-MRI is performed in combination with T2-weighted imaging (with or without the addition of contrast enhancement) suggests that preoperative imaging may be able to differentiate between the 2 categories of bladder cancer, which in selected patients may have a clinical impact[30] (Fig. 4).

The prognosis of bladder tumours correlates inversely with the histological grading. The ADC may in part predict the histological grade of a bladder cancer, as observed in a recent study[30], which demonstrated that the mean ADCs of G1, G2, and G3 tumours were $(1.29 \pm 0.21) \times 10^{-3}$ mm^2/s, $(1.13 \pm 0.24) \times 10^{-3}$ mm^2/s and $(0.81 \pm 0.11) \times 10^{-3}$ mm^2/s, respectively, with significantly lower ADC values for G3 tumours compared with G1 ($P < 0.01$) and to G2 ($P < 0.01$)

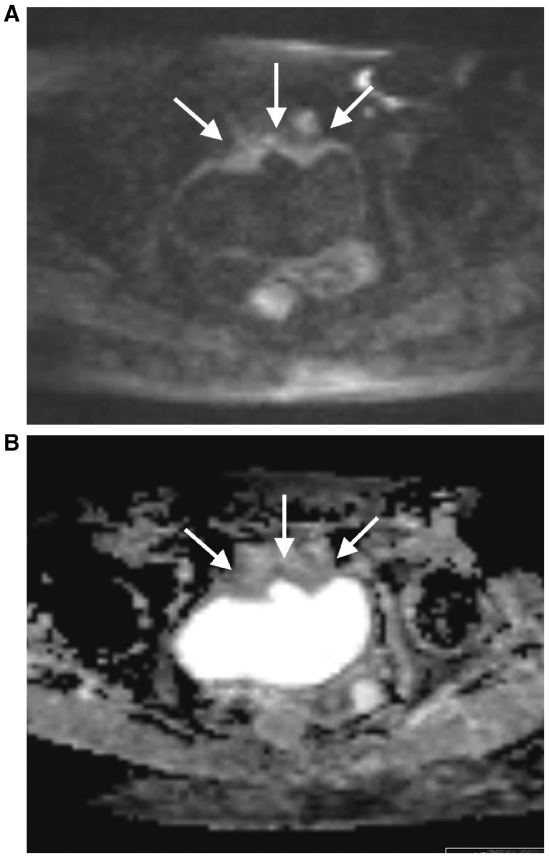

Figure 4 **MRI (at 3 T) of a 69-year-old female patient with a pT3 TCC of the bladder. (A) On the DW-MR image at a *b* value of 1000 s/mm^2 the tumour is seen as thickening of the anterior bladder wall with high signal intensity and with irregular outer margins extending into the surrounding fat tissue (arrows). (B) On the corresponding ADC map the tumour is visualized as thickening of the bladder wall with impeded diffusion, represented by colour shades of dark grey (arrows).**

tumours. In addition, DW-MRI in patients with bladder cancer may detect bone metastases not diagnosed on scintigraphy.

Prostate

When a prostate cancer reaches the size of so-called significant disease (>0.5 mL), corresponding to a diameter of 10 mm, it is expected to produce 1.75 ng/mL of prostate-specific antigen (PSA), since it is known that 1 g of prostate cancer produces 3.5 ng/mL of PSA. However, benign prostatic hyperplasia (BPH) as well as normal prostatic tissue contributes to the total PSA, producing 0.3 ng/mL and 0.1 ng/mL of PSA per gram, respectively. Therefore it is difficult to reliably predict prostate cancer based on PSA level alone[31]. In a study from Thompson *et al.*[32], 15.2% of men with a PSA level $\leq$4.0 ng/mL had prostate cancer. Another study demonstrated prostate cancer was detected in only 32% of those with a PSA

level between 4 and 10 ng/mL and in 41% of men with a PSA level between 10.1 and 20 ng/mL[33].

Thus, even a PSA level <10 ng/ml does not discriminate between prostate cancer and other prostate pathologies, such as, for example, prostatitis or BPH. The diagnosis of prostate cancer is still based mostly on the results of ultrasonography (US)-guided transrectal biopsy, performed with multiple random samples, as the low accuracy of US for prostate cancer detection and localization often does not allow a targeted biopsy. Advances in imaging are therefore of utmost importance for the diagnosis of prostate cancer and for its localization.

Because of the intrinsic low contrast resolution, CT is not adequate for the assessment of organ-confined prostate cancers. MRI using T2-weighted imaging has been used for the work-up of prostate cancer, but is limited because of unsatisfactory sensitivity and specificity for prostate cancer detection and localization, especially when the cancer is located in the transitional and central zones, because cancer and normal tissues both have low signal intensity on T2-weighted images. Furthermore, differentiation between tumour and prostatitis is often not possible.

Various other MR techniques have been applied for prostate cancer imaging. Dynamic contrast-enhanced magnetic resonance imaging (DCE-MRI) is based on the concept that tumours present different vascularity as a result of the angiogenic process compared with background parenchyma. DCE-MRI has been used for tumour localization[34], for the evaluation of tumour vascularity[35], as well as for the discrimination of prostate cancer in the PZ from normal PZ tissue, and stromal and glandular BPH[36]. Some authors have observed better performances of DCE-MRI compared with T2-weighted imaging in tumour detection at 1.5 T[35] and at 3 T[37,38].

Proton (^{1}H) MR spectroscopic imaging (MRSI) has also been used for prostate cancer work-up. The detection of prostate cancer has been based primarily on the identification of an increased choline-to-citrate ratio, or, for practical purposes, the choline plus the creatine (Cho+Cr)/citrate ratio. The use of combined MRI/MRSI is generally considered to improve the specificity of prostate cancer detection and it may also be useful for risk stratification of prostate cancers[38,39]. However, in a recent multicentric study the accuracy of combined imaging including endorectal MRI and MRSI at 1.5 T for the sextant localization of prostate cancer in the PZ was found to be comparable with that of T2-weighted MRI alone[40]. Such a modest performance of MRSI could also be explained by the difficulty of the technique, requiring experience in data acquisition and interpretation.

Although DCE-MRI and ^{1}H MR spectroscopy have shown promise both for tumour detection and characterization, neither method provides image resolution sufficient for practical tumour localization[41–43].

DW-MRI is feasible on the prostate and the calculation of the ADC values is relatively straightforward. In the prostate tissue, the predominant contribution of the extracellular component is from tubular structures and their fluid content, whereas the intracellular component is determined by the epithelial and stromal cells.

In most cases, the PZ can be easily discriminated from the central gland (CG), because it displays relatively higher ADC values compared with the PZ[44–47]. The CG consists of more compact smooth muscle cells and sparser glandular elements than the PZ, leading to a lower extracellular-to-intracellular fluid ratio and to lower ADC values. Prostate carcinoma is histologically characterized by a higher cellular density than normal prostate tissue, with replacement of the normal glandular tissue; thus, it is expected to show a more impeded diffusion of water molecules, compared with normal prostatic gland[48,49].

Several studies have demonstrated significantly lower ADC values in prostate carcinoma compared with benign prostatic tissue[50–53], suggesting clinical utility in prostate cancer detection. In particular, the addition of DW-MRI to T2-weighted MRI has been shown to improve the detection of prostatic carcinoma in the PZ[54], as a result of the contrast between the low ADC values of the prostate carcinoma and the relatively high ADC values of the PZ, in which tumours occur in 70% of cases[55] (Fig. 5).

The addition of DW-MRI to T2-weighted MRI also provides a definitely higher spatial resolution than MRSI and DCE-MRI. A close correlation between DW-MRI and histology has been demonstrated in a study by Xu *et al.*[56] for the visualization of prostate cancer. Similar results were reported in a study showing that the addition of DW-MRI to T2-weighted imaging can significantly improve the accuracy of prostate PZ tumour volume measurements[57]. The results of the above-mentioned studies showed the ability of DW-MRI to image prostate cancers when they are larger than 0.1 cm^3, suggesting its potential role for prostate cancer localization, when it is located in the PZ.

However, detection and localization of prostate carcinoma in the CG remain challenging, as there is an overlap in ADC values between tumour and BPH. In these cases, diffusion tensor imaging (DTI), which allows for the evaluation of tissue anisotropy, is showing promise.

Fractional anisotropy (FA) is determined along the axis of the tubular structures of normal prostate tissue. High FA is generally observed in stromal BPH, thus avoiding false-positive identification of a prostate carcinoma in the CG; FA is reduced[50,58] in prostate carcinoma, as a result of the destruction of tubular structures. DTI has therefore the potential to provide information on prostate microstructure at a micrometre scale, but further clinical studies are needed to identify its role in prostate cancer imaging.

Preliminary studies have been published recently, evaluating the prognostic value of ADC in prostate tumours.

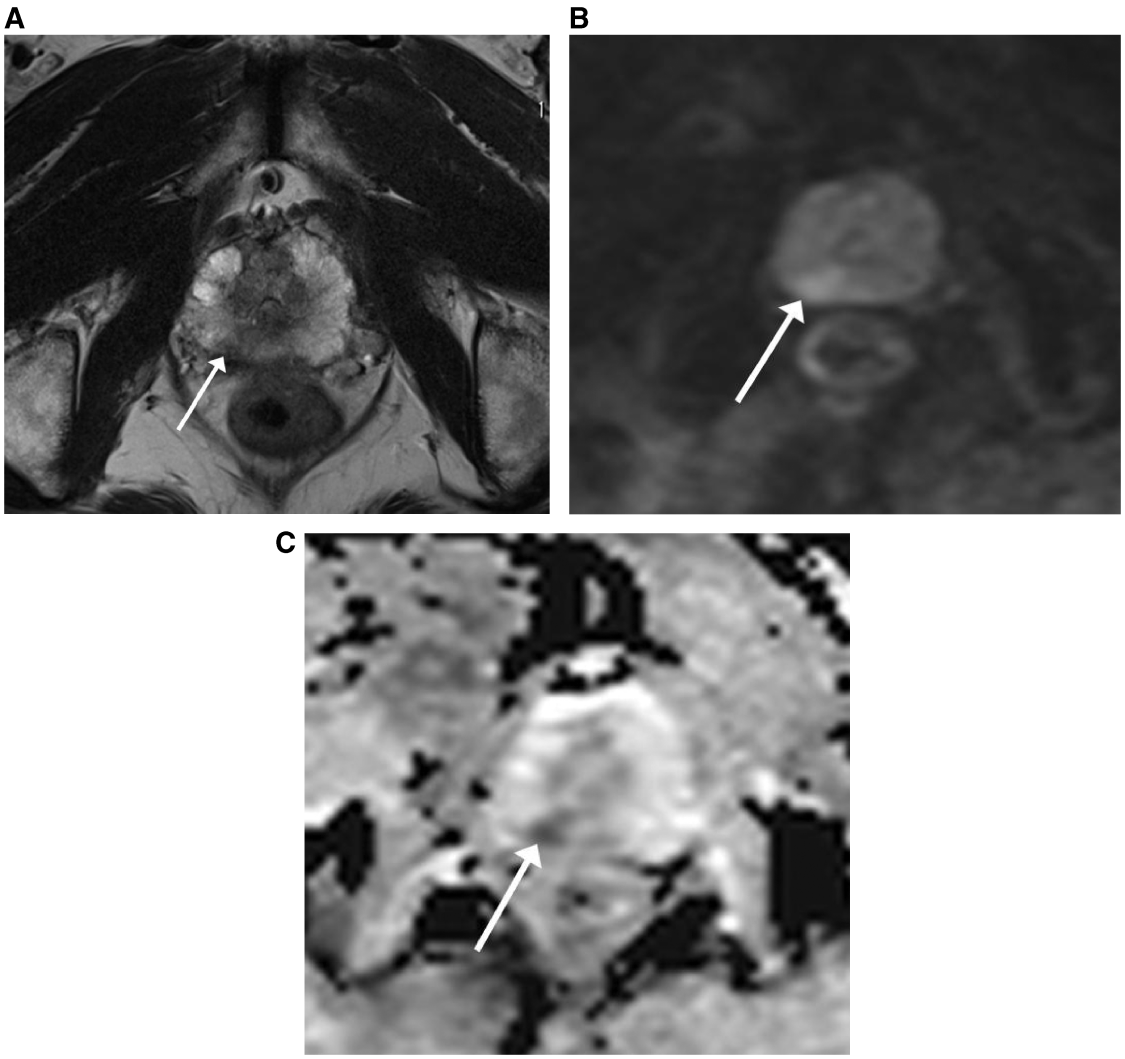

Figure 5 **MRI (at 3 T) of a 69-year-old patient with a prostate carcinoma in the PZ on the right side (arrow). (A) On the axial T2-weighted MR image the tumour is visualized as an area of low signal intensity (arrow). (B) On the DW-MR image at a *b* value of 1000 s/mm^2 the tumour is not clearly visualized because of the T2 shine-through effect in the PZ of the prostate. (C) On the ADC map the tumour is clearly visualized as an area of impeded diffusion, represented by colour shades of dark grey, in contrast with the normal PZ of the prostate, which returns colour shades of light grey.**

Both ADC values calculated with *b* values from 0 to 100 and with *b* values from 100 to 800 s/mm^2 were found to be significantly lower in patients with higher risk compared with those with low risk localized prostate cancer[59]. In patients with untreated localized prostate cancer on active surveillance, low tumour ADC values were associated with adverse histology on repeat biopsy and shorter time to deferred radical treatment[60].

There is a short experience in treatment monitoring of prostate tumours by DW-MRI. To the best of our knowledge, there is only one study on humans that used DW-MRI for monitoring carbon-ion radiotherapy, which demonstrated a significant increase in tumour ADC values after therapy (3–9 months after treatment); no changes in the non-cancerous inner gland (IG) and in the PZ[61] were observed. DW-MRI has also been applied for early monitoring of thermal therapy in canine normal prostate. In the treated area authors observed a decrease in ADC values a few days after thermal therapy and an increase over time as the treated area recovered and regenerated[62]. These studies showed that DW-MRI might also have a role for monitoring non-surgical therapies in prostate cancer. However, further studies are required to identify a role for DW-MRI with respect to predicting clinical outcomes and treatment monitoring.

To the best of our knowledge, there is only one study that investigated the role of DW-MRI in recurrent prostate cancer[63]. This study showed that DW-MRI, when added to T2-weighted imaging, improved the ability to discriminate between recurrent disease and post-therapeutic changes in patients who have received radiotherapy treatment. These encouraging results suggest a

validation of the role of DW-MRI for recurrent prostate carcinoma on a larger scale, as an earlier diagnosis and a more accurate intraprostatic mapping of the recurred prostate cancer after radiation therapy can provide better selection of the appropriate second-line treatment.

Lymph nodes

Lymph node staging in patients with bladder or prostate tumours is based on size criteria only when performing conventional cross-sectional imaging, such as CT and MR. This may not be adequate for staging such tumours, because micrometastases are demonstrated in about 25% of patients with preoperatively negative normal-sized lymph nodes on imaging studies[64,65]. In addition, it has been demonstrated that the incidence of positive lymph nodes is higher in patients with a Gleason score ≥ 7 (25%) compared with those with a Gleason score <6 (3%)[66], and that the survival is significantly better in the absence of lymph node involvement in patients with bladder cancer. Thus, there is an urgent need for an improvement in the diagnosis of malignant lymph nodes by preoperative imaging.

DW-MRI may have a role in the assessment of malignant lymph nodes from urogenital tumours, because malignant nodes are in theory expected to show impeded diffusion, resulting in low ADC values, as most primary malignant tumours show impeded diffusion caused by high cellularity (Fig. 6). There is one study including 29 patients that investigated the potential contribution of ADC values in the differentiation between benign and malignant lymph nodes in patients with prostate cancer, showing significant differences in the mean ADC for b values of 50, 300, and 600 s/mm^2 between malignant ($1.07 \pm 0.23 \times 10^{-3}$ mm^2/s) and benign ($1.54 \pm 0.25 \times 10^{-3}$ mm^2/s) lymph nodes[67]. However, definitive data are not yet available and the potential of DW-MRI for lymph node assessment in normal-sized nodes is still being investigated.

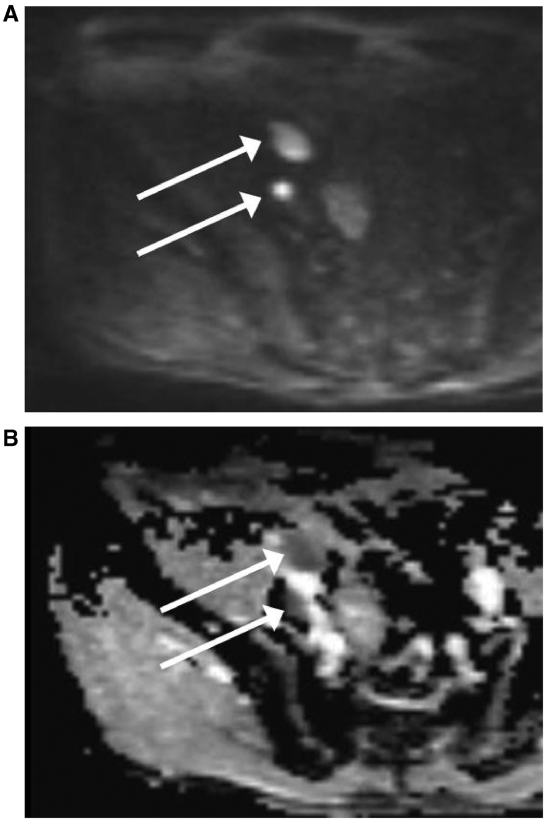

Figure 6 **MRI (at 3 T) of a 50-year-old patient with 2 lymph node metastases from prostate carcinoma in the right external iliac chain. (A) On the DW-MR image at a b value of 1000 s/mm^2 the lymph node metastases show high signal intensity (arrows). (B) On the corresponding ADC map the lymph node metastases reveal impeded diffusion, represented by colour shades of dark grey.**

Future challenges

The lack of standardization in imaging technique and analysis is one of the most important shortcomings of DW-MRI, which slightly hampers its use in clinical practice and limits comparison between studies. The use of DW-MR sequences with different parameters, as well as the use of different field strengths and MR scanners from different manufacturers may raise variability in the qualitative and quantitative assessment of DW-MRI. Therefore identical parameters of DW-MR sequences are a prerequisite to perform longitudinal studies and to compare results with those published in the literature[7,68]. Efforts have been conducted in the last few years to standardize DW-MRI sequences and image analysis[69,70]; however, there is still a lack of official guidelines from the major scientific societies, which may contribute to expand this knowledge to a wider community, including newcomers and clinicians.

First goals would be standardization of image acquisition and sequences across multiple scanner platforms in multiple institutions, accounting for equipment variability as well as for the differences in imaging practice across different sites. Then, reading/analysis bias must be controlled in the qualitative and quantitative analysis of DW-MRI. The achievement of these goals would permit multisite clinical trials, which are required for a definitive validation of such a technique in the assessment of urogenital tract tumours.

Other goals would be to explore the potential of DW-MRI for tumours of the urogenital tract as a biomarker in clinical practice, able to influence patient management, or in drug development, providing insights into the efficacy and/or toxicity of a compound. For example, anti-angiogenic therapy, including tyrosine kinase inhibitors (sunitinib and sorafenib), bevacizumab with interferon alpha, temsirolimus, and everolimus, is increasingly used for metastatic RCC[71]. As these new agents

do not lead to an immediate size reduction of the tumour, newer imaging techniques providing microstructural information are warranted.

DW-MRI has been shown to be able to demonstrate changes prior to alterations in tumour size after drug treatment and has thus been proposed as a potential biomarker of early drug activity. On the other hand, there are now multiple early-phase clinical trials of anti-angiogenic agents in prostate cancer[72]. A biomarker for estimating the optimal dose and scheduling is therefore required; there are preliminary experiences reporting the potential of DW-MRI to provide such an evaluation, providing different ADC values at different dose levels and days of therapy[73]. However, the validation of DW-MRI as a biomarker in drug development is linked to its integration into a platform of multifunctional MR imaging.

Improvements in lymph node imaging are necessary. Further efforts are needed to explore the potential of DW-MRI (eventually in combination with ultrasmall superparamagnetic iron oxide-enhanced MRI) to detect lymph node metastases even in normal-sized lymph nodes[74] and to differentiate between enlarged reactive nodes and metastases in RCC, for example.

Conclusion

Although MR and CT are excellent imaging modalities in the diagnostic work-up of several urogenital tumours, DW-MRI is showing promising results as a non-invasive and sensitive technique to provide information one step beyond morphology. Therefore, DW-MRI merits further studies to validate its potential for application in tumours of the urogenital tract in larger scale studies.

Acknowledgement

This work was supported by research grant no. 320000–113512 of the Swiss National Science Foundation for Research and Carigest SA, Geneva.

References

[1] Moseley ME, Cohen Y, Mintorovitch J, *et al.* Early detection of regional cerebral ischemia in cats: comparison of diffusion- and T2-weighted MRI and spectroscopy. Magn Reson Med 1990; 14: 330–46. doi:10.1002/mrm.1910140218. PMid:2345513.

[2] Schaefer PW, Grant PE, Gonzalez RG. Diffusion-weighted MR imaging of the brain. Radiology 2000; 217: 331–45.

[3] Johnston KC, Wagner DP, Wang XQ, *et al.* Validation of an acute ischemic stroke model: does diffusion-weighted imaging lesion volume offer a clinically significant improvement in prediction of outcome? Stroke 2007; 38: 1820–5. doi:10.1161/STROKEAHA.106.479154. PMid:17446421.

[4] Murtz P, Flacke S, Traber F, van den Brink JS, Gieseke J, Schild HH. Abdomen: diffusion-weighted MR imaging with pulse-triggered single-shot sequences. Radiology 2002; 224: 258–64. doi:10.1148/radiol.2241011117. PMid:12091693.

[5] Thoeny HC, De Keyzer F. Extracranial applications of diffusion-weighted magnetic resonance imaging. Eur Radiol 2007; 17: 1385–93. doi:10.1007/s00330-006-0547-0. PMid:17206421.

[6] Le Bihan D, Breton E, Lallemand D, Aubin ML, Vignaud J, Laval-Jeantet M. Separation of diffusion and perfusion in intravoxel incoherent motion MR imaging. Radiology 1988; 168: 497–505.

[7] Thoeny HC, De Keyzer F, Boesch C, Hermans R. Diffusion-weighted imaging of the parotid gland: Influence of the choice of b-values on the apparent diffusion coefficient value. J Magn Reson Imaging 2004; 20: 786–90. doi:10.1002/jmri.20196. PMid:15503336.

[8] Lyng H, Haraldseth O, Rofstad EK. Measurement of cell density and necrotic fraction in human melanoma xenografts by diffusion weighted magnetic resonance imaging. Magn Reson Med 2000; 43: 828–36. doi:10.1002/1522-2594(200006)43:6<828::AID-MRM8>3.0.CO;2-P.

[9] Kim S, Naik M, Sigmund E, Taouli B. Diffusion-weighted MR imaging of the kidneys and the urinary tract. Magn Reson Imaging Clin N Am 2008; 16: 585–96. doi:10.1016/j.mric.2008.07.006. PMid:18926424.

[10] Koh DM, Collins DJ. Diffusion-weighted MRI in the body: applications and challenges in oncology. AJR Am J Roentgenol 2007; 188: 1622–35. doi:10.2214/AJR.06.1403. PMid:17515386.

[11] Squillaci E, Manenti G, Di Stefano F, Miano R, Strigari L, Simonetti G. Diffusion-weighted MR imaging in the evaluation of renal tumours. J Exp Clin Cancer Res 2004; 23: 39–45.

[12] Cova M, Squillaci E, Stacul F, *et al.* Diffusion-weighted MRI in the evaluation of renal lesions: preliminary results. Br J Radiol 2004; 77: 851–7. doi:10.1259/bjr/26525081. PMid:15482997.

[13] Zhang J, Tehrani YM, Wang L, Ishill NM, Schwartz LH, Hricak H. Renal masses: characterization with diffusion-weighted MR imaging–a preliminary experience. Radiology 2008; 247: 458–64. doi:10.1148/radiol.2472070823. PMid:18430878.

[14] Taouli B, Thakur RK, Mannelli L, *et al.* Renal lesions: characterization with diffusion-weighted imaging versus contrast-enhanced MR imaging. Radiology 2009; 251: 398–407. doi:10.1148/radiol.2512080880. PMid:19276322.

[15] Grobner T. Gadolinium–a specific trigger for the development of nephrogenic fibrosing dermopathy and nephrogenic systemic fibrosis? Nephrol Dial Transplant 2006; 21: 1104–8. doi:10.1093/ndt/gfk062. PMid:16431890.

[16] Sadowski EA, Bennett LK, Chan MR, *et al.* Nephrogenic systemic fibrosis: risk factors and incidence estimation. Radiology 2007; 243: 148–57. doi:10.1148/radiol.2431062144. PMid:17267695.

[17] Boyd AS, Zic JA, Abraham JL. Gadolinium deposition in nephrogenic fibrosing dermopathy. J Am Acad Dermatol 2007; 56: 27–30. doi:10.1016/j.jaad.2006.10.048. PMid:17109993.

[18] Morcos SK, Thomsen HS, Webb JA. Contrast-media-induced nephrotoxicity: a consensus report. Contrast Media Safety Committee, European Society of Urogenital Radiology (ESUR). Eur Radiol 1999; 9: 1602–13. doi:10.1007/s003300050894. PMid:10525875.

[19] Mehran R, Nikolsky E. Contrast-induced nephropathy: definition, epidemiology, and patients at risk. Kidney Int 2006(Suppl): S11–5.

[20] Kim S, Jain M, Harris AB, *et al.* T1 hyperintense renal lesions: characterization with diffusion-weighted MR imaging versus contrast-enhanced MR imaging. Radiology 2009; 251: 796–807. doi:10.1148/radiol.2513080724. PMid:19380690.

[21] Bradford TJ, Montie JE, Hafez KS. The role of imaging in the surveillance of urologic malignancies. Urol Clin North Am 2006; 33: 377–96. doi:10.1016/j.ucl.2006.03.001. PMid:16829272.

[22] Kaufman DS. Challenges in the treatment of bladder cancer. Ann Oncol 2006; 17(Suppl 5): v106–12. doi:10.1093/annonc/mdj963. PMid:16807436.

[23] Ng CS. Radiologic diagnosis and staging of renal and bladder cancer. Semin Roentgenol 2006; 41: 121–38. doi:10.1053/j.ro.2006.02.005. PMid:16697891.

[24] Josephson D, Pasin E, Stein JP. Superficial bladder cancer: part 2. Management. Expert Rev Anticancer Ther 2007; 7: 567–81. doi:10.1586/14737140.7.4.567. PMid:17428176.
[25] Sherif A, Jonsson MN, Wiklund NP. Treatment of muscle-invasive bladder cancer. Expert Rev Anticancer Ther 2007; 7: 1279–83. doi:10.1586/14737140.7.9.1279. PMid:17892428.
[26] Herr HW. The value of a second transurethral resection in evaluating patients with bladder tumors. J Urol 1999; 162: 74–6. doi:10.1097/00005392-199907000-00018. PMid:10379743.
[27] Vikram R, Sandler CM, Ng CS. Imaging and staging of transitional cell carcinoma: part 1, lower urinary tract. AJR Am J Roentgenol 2009; 192: 1481–7. doi:10.2214/AJR.08.1318. PMid:19457808.
[28] El-Assmy A, Abou-El-Ghar ME, Mosbah A, *et al.* Bladder tumour staging: comparison of diffusion- and T2-weighted MR imaging. Eur Radiol 2009; 19: 1575–81. doi:10.1007/s00330-009-1340-7. PMid:19247665.
[29] Watanabe H, Kanematsu M, Kondo H, *et al.* Preoperative T staging of urinary bladder cancer: does diffusion-weighted MRI have supplementary value? AJR Am J Roentgenol 2009; 192: 1361–6. doi:10.2214/AJR.08.1430. PMid:19380561.
[30] Takeuchi M, Sasaki S, Ito M, *et al.* Urinary bladder cancer: diffusion-weighted MR imaging–accuracy for diagnosing T stage and estimating histologic grade. Radiology 2009; 251: 112–21. doi:10.1148/radiol.2511080873. PMid:19332849.
[31] Thompson IM, Ankerst DP, Chi C, *et al.* Assessing prostate cancer risk: results from the Prostate Cancer Prevention Trial. J Natl Cancer Inst 2006; 98: 529–34.
[32] Thompson IM, Pauler DK, Goodman PJ, *et al.* Prevalence of prostate cancer among men with a prostate-specific antigen level < or = 4.0 ng per milliliter. N Engl J Med 2004; 350: 2239–46. doi:10.1056/NEJMoa031918. PMid:15163773.
[33] Carlson GD, Calvanese CB, Partin AW. An algorithm combining age, total prostate-specific antigen (PSA), and percent free PSA to predict prostate cancer: results on 4298 cases. Urology 1998; 52: 455–61. doi:10.1016/S0090-4295(98)00205-2.
[34] Futterer JJ, Heijmink SW, Scheenen TW, *et al.* Prostate cancer localization with dynamic contrast-enhanced MR imaging and proton MR spectroscopic imaging. Radiology 2006; 241: 449–58. doi:10.1148/radiol.2412051866. PMid:16966484.
[35] Buckley DL, Roberts C, Parker GJ, Logue JP, Hutchinson CE. Prostate cancer: evaluation of vascular characteristics with dynamic contrast-enhanced T1-weighted MR imaging–initial experience. Radiology 2004; 233: 709–15. doi:10.1148/radiol.2333032098. PMid:15498903.
[36] Noworolski SM, Henry RG, Vigneron DB, Kurhanewicz J. Dynamic contrast-enhanced MRI in normal and abnormal prostate tissues as defined by biopsy, MRI, and 3D MRSI. Magn Reson Med 2005; 53: 249–55. doi:10.1002/mrm.20374. PMid:15678552.
[37] Kim CK, Park BK, Kim B. Localization of prostate cancer using 3T MRI: comparison of T2-weighted and dynamic contrast-enhanced imaging. J Comput Assist Tomogr 2006; 30: 7–11. doi:10.1097/01.rct.0000185384.27765.09. PMid:16365565.
[38] Shukla-Dave A, Hricak H, Kattan MW, *et al.* The utility of magnetic resonance imaging and spectroscopy for predicting insignificant prostate cancer: an initial analysis. BJU Int 2007; 99: 786–93. doi:10.1111/j.1464-410X.2007.06689.x. PMid: 17223922.
[39] Coakley FV, Chen I, Qayyum A, *et al.* Validity of prostate-specific antigen as a tumour marker in men with prostate cancer managed by watchful-waiting: correlation with findings at serial endorectal magnetic resonance imaging and spectroscopic imaging. BJU Int 2007; 99: 41–5. doi:10.1111/j.1464-410X.2006.06515.x. PMid:17227490.
[40] Weinreb JC, Blume JD, Coakley FV, *et al.* Prostate cancer: sextant localization at MR imaging and MR spectroscopic imaging before prostatectomy – results of ACRIN prospective multi-institutional clinicopathologic study. Radiology 2009; 251: 122–33. doi:10.1148/radiol.2511080409. PMid:19332850.
[41] Coakley FV, Qayyum A, Kurhanewicz J. Magnetic resonance imaging and spectroscopic imaging of prostate cancer. J Urol 2003; 170: S69–75; discussion S75–66. doi:10.1097/01.ju.0000094958.23276.c4. PMid:14610414.
[42] Padhani AR, Gapinski CJ, Macvicar DA, *et al.* Dynamic contrast enhanced MRI of prostate cancer: correlation with morphology and tumour stage, histological grade and PSA. Clin Radiol 2000; 55: 99–109. doi:10.1053/crad.1999.0327. PMid:10657154.
[43] Xu J, Does MD, Gore JC. Sensitivity of MR diffusion measurements to variations in intracellular structure: effects of nuclear size. Magn Reson Med 2009; 61: 828–33. doi:10.1002/mrm.21793. PMid:19205020.
[44] Kim CK, Park BK, Lee HM, Kwon GY. Value of diffusion-weighted imaging for the prediction of prostate cancer location at 3T using a phased-array coil: preliminary results. Invest Radiol 2007; 42: 842–7. doi:10.1097/RLI.0b013e3181461d21. PMid: 18007156.
[45] Kumar V, Jagannathan NR, Kumar R, *et al.* Apparent diffusion coefficient of the prostate in men prior to biopsy: determination of a cut-off value to predict malignancy of the peripheral zone. NMR Biomed 2007; 20: 505–11. doi:10.1002/nbm.1114. PMid:17167820.
[46] Tamada T, Sone T, Jo Y, *et al.* Apparent diffusion coefficient values in peripheral and transition zones of the prostate: comparison between normal and malignant prostatic tissues and correlation with histologic grade. J Magn Reson Imaging 2008; 28: 720–6. doi:10.1002/jmri.21503. PMid:18777532.
[47] Tamada T, Sone T, Toshimitsu S, *et al.* Age-related and zonal anatomical changes of apparent diffusion coefficient values in normal human prostatic tissues. J Magn Reson Imaging 2008; 27: 552–6. doi:10.1002/jmri.21117. PMid:18219616.
[48] Anderson AW, Xie J, Pizzonia J, Bronen RA, Spencer DD, Gore JC. Effects of cell volume fraction changes on apparent diffusion in human cells. Magn Reson Imaging 2000; 18: 689–95. doi:10.1016/S0730-725X(00)00147-8.
[49] Song SK, Qu Z, Garabedian EM, Gordon JI, Milbrandt J, Ackerman JJ. Improved magnetic resonance imaging detection of prostate cancer in a transgenic mouse model. Cancer Res 2002; 62: 1555–8.
[50] Gibbs P, Pickles MD, Turnbull LW. Diffusion imaging of the prostate at 3.0 tesla. Invest Radiol 2006; 41: 185–8. doi:10.1097/01.rli.0000192418.30684.14. PMid:16428991.
[51] Hosseinzadeh K, Schwarz SD. Endorectal diffusion-weighted imaging in prostate cancer to differentiate malignant and benign peripheral zone tissue. J Magn Reson Imaging 2004; 20: 654–61. doi:10.1002/jmri.20159. PMid:15390142.
[52] Shimofusa R, Fujimoto H, Akamata H, *et al.* Diffusion-weighted imaging of prostate cancer. J Comput Assist Tomogr 2005; 29: 149–53. doi:10.1097/01.rct.0000156396.13522.f2. PMid:15772529.
[53] Haider MA, van der Kwast TH, Tanguay J, *et al.* Combined T2-weighted and diffusion-weighted MRI for localization of prostate cancer. AJR Am J Roentgenol 2007; 189: 323–8. doi:10.2214/AJR.07.2211. PMid:17646457.
[54] Morgan VA, Kyriazi S, Ashley SE, DeSouza NM. Evaluation of the potential of diffusion-weighted imaging in prostate cancer detection. Acta Radiol 2007; 48: 695–703. doi:10.1080/02841850701349257. PMid:17611881.
[55] Choi YJ, Kim JK, Kim N, Kim KW, Choi EK, Cho KS. Functional MR imaging of prostate cancer. Radiographics 2007; 27: 63–75; discussion 75–67. doi:10.1148/rg.271065078. PMid:17234999.
[56] Xu J, Humphrey PA, Kibel AS, *et al.* Magnetic resonance diffusion characteristics of histologically defined prostate cancer in humans. Magn Reson Med 2009; 61: 842–50. doi:10.1002/mrm.21896. PMid:19215051.

[57] Mazaheri Y, Hricak H, Fine SW, *et al.* Prostate tumor volume measurement with combined T2-weighted imaging and diffusion-weighted MR: correlation with pathologic tumor volume. Radiology 2009; 252: 449–57. doi:10.1148/radiol.2523081423. PMid:19703883.

[58] Manenti G, Carlani M, Mancino S, *et al.* Diffusion tensor magnetic resonance imaging of prostate cancer. Invest Radiol 2007; 42: 412–9. doi:10.1097/01.rli.0000264059.46444.bf. PMid: 17507813.

[59] deSouza NM, Riches SF, Vanas NJ, *et al.* Diffusion-weighted magnetic resonance imaging: a potential non-invasive marker of tumour aggressiveness in localized prostate cancer. Clin Radiol 2008; 63: 774–82. doi:10.1016/j.crad.2008.02.001. PMid:18555035.

[60] van As NJ, de Souza NM, Riches SF, *et al.* A study of diffusion-weighted magnetic resonance imaging in men with untreated localised prostate cancer on active surveillance. Eur Urol 2008; 56: 981–8. doi:10.1016/j.eururo.2008.11.051. PMid:19095345.

[61] Takayama Y, Kishimoto R, Hanaoka S, *et al.* ADC value and diffusion tensor imaging of prostate cancer: changes in carbon-ion radiotherapy. J Magn Reson Imaging 2008; 27: 1331–5. doi:10.1002/jmri.21388. PMid:18504751.

[62] Chen J, Daniel BL, Diederich CJ, *et al.* Monitoring prostate thermal therapy with diffusion-weighted MRI. Magn Reson Med 2008; 59: 1365–72. doi:10.1002/mrm.21589. PMid:18506801.

[63] Kim CK, Park BK, Lee HM. Prediction of locally recurrent prostate cancer after radiation therapy: incremental value of 3T diffusion-weighted MRI. J Magn Reson Imaging 2009; 29: 391–7. doi:10.1002/jmri.21645. PMid:19161194.

[64] Fleischmann A, Thalmann GN, Markwalder R, Studer UE. Extracapsular extension of pelvic lymph node metastases from urothelial carcinoma of the bladder is an independent prognostic factor. J Clin Oncol 2005; 23: 2358–65. doi:10.1200/JCO.2005.03.084. PMid:15800327.

[65] Bader P, Burkhard FC, Markwalder R, Studer UE. Disease progression and survival of patients with positive lymph nodes after radical prostatectomy. Is there a chance of cure? J Urol 2003; 169: 849–54.

[66] Schumacher MC, Burkhard FC, Thalmann GN, Fleischmann A, Studer UE. Is pelvic lymph node dissection necessary in patients with a serum PSA <10 ng/ml undergoing radical prostatectomy for prostate cancer? Eur Urol 2006; 50: 272–9. doi:10.1016/j.eururo.2006.01.061. PMid:16632187.

[67] Eiber M, Beer AJ, Holzapfel K, *et al.* Preliminary results for characterization of pelvic lymph nodes in patients with prostate cancer by diffusion-weighted MR-imaging. Invest Radiol 2010; 45: 15–23. doi:10.1097/RLI.0b013e3181bbdc2f. PMid:19996762.

[68] Dale BM, Braithwaite AC, Boll DT, Merkle EM. Field strength and diffusion encoding technique affect the apparent diffusion coefficient measurements in diffusion-weighted imaging of the abdomen. Invest Radiol 2010; 45: 104–8. doi:10.1097/RLI.0b013e3181c8ceac. PMid:20027117.

[69] Padhani AR, Liu G, Koh DM, *et al.* Diffusion-weighted magnetic resonance imaging as a cancer biomarker: consensus and recommendations. Neoplasia 2009; 11: 102–25.

[70] Thoeny HC, Ross BD. Predicting and monitoring cancer treatment response with diffusion-weighted MRI. J Magn Reson Imaging 2010; 32: 2–16. doi:10.1002/jmri.22167. PMid: 20575076.

[71] Hutson TE, Figlin RA. Novel therapeutics for metastatic renal cell carcinoma. Cancer 2009; 115: 2361–7. doi:10.1002/cncr.24235. PMid:19402059.

[72] Kluetz PG, Figg WD, Dahut WL. Angiogenesis inhibitors in the treatment of prostate cancer. Expert Opin Pharmacother 2010; 11: 233–47. doi:10.1517/14656560903451716. PMid:20088745.

[73] Hamstra DA, Chenevert TL, Moffat BA, *et al.* Evaluation of the functional diffusion map as an early biomarker of time-to-progression and overall survival in high-grade glioma. Proc Natl Acad Sci U S A 2005; 102: 16759–64. doi:10.1073/pnas.0508347102. PMid:16267128.

[74] Thoeny HC, Triantafyllou M, Birkhaeuser FD, *et al.* Combined ultrasmall superparamagnetic particles of iron oxide-enhanced and diffusion-weighted magnetic resonance imaging reliably detect pelvic lymph node metastases in normal-sized nodes of bladder and prostate cancer patients. Eur Urol 2009; 55: 761–9. doi:10.1016/j.eururo.2008.12.034. PMid:19144456.